Journal of Hydroinformatics

Journal of Hydroinformatics Vol 25 No 3, 1004 doi: 10.2166/hydro.2023.212

ANFIS- and GEP-based model for prediction of scour depth around bridge pier in clear-water scouring and live-bed scouring conditions

Amandeep Choudhary [a], Bhabani Shankar Das [a,*], Kamalini Devi [b] and Jnana Ranjan Khuntia [b]

[a] Civil Engineering Department, National Institute of Technology, Patna, India
[b] Civil Engineering Department, Chaitanya Bharathi Institute of Technology, Hyderabad, India
*Corresponding author. E-mail: bsd.nitrkl@gmail.com

AC, 0000-0003-3889-951X; BSD, 0000-0003-1140-0432; KD, 0000-0002-5916-3256; JRK, 0000-0003-3943-4220

ABSTRACT

Scour depth prediction is an important aspect of designing a bridge pier structure in a river. Proper modeling of scour depth ensures the sustainability of the structure. An attempt is made to develop a scour depth model for the bridge pier using an adaptive network-based fuzzy inference system (ANFIS) and gene expression programming (GEP). The scour depth is found to be influenced by various independent parameters such as pier diameter, flow depth, approach mean velocity, critical velocity, Froude number, bed sediment, and geometric standard deviation of bed particle size. Gamma tests are performed to identify the best input parameter combinations to predict scour depth. In the present study, two separate models have been developed for clear-water scouring (CWS) and live-bed scouring (LBS). For different ranges of input parameters, the scour depth ratio is computed and error analysis is performed. Results indicate that the ANFIS model ($R^2_{CWS} = 0.95$, $MAPE_{CWS} = 9.39\%$ and $R^2_{LBS} = 0.95$, $MAPE_{LBS} = 5.29\%$) is the most accurate predictive model in both scour conditions as compared to the GEP model and existing models of previous researchers. However, for the low value of pier diameter (b) to flow depth (y) ratio (<0.25), the present ANFIS model apportioned unsatisfactory results for LBS only.

Key words: ANFIS, clear-water scouring, GEP, scour depth, live-bed scouring

HIGHLIGHTS

- Separate models have been proposed for clear-water scouring and live-bed scouring of bridge piers using ANFIS and GEP.
- The influencing parameters affecting the scour depth are identified using the Gamma test.
- A wide range of data is considered in developing a model for scour depth around bridge piers.
- The performance of the scour depth models is evaluated for various ranges of input parameters such as b/y, U/U_c, and Fr.

NOMENCLATURE

μ	fluid dynamic viscosity
b	pier diameter
d_{50}	median diameter of sediment
d_{se}	scour depth
F_{d50}	particle densiometric Froude number
Fr	Froude number
F_{rc}	critical Froude number
g	acceleration due to gravity
U	approach mean velocity
U_c	critical velocity
y	flow depth
ρ	fluid density
σ	geometric standard deviation of bed sediment size

ABBREVIATIONS

ANFIS	adaptive network-based fuzzy inference system
ANN	artificial neural network
CWS	clear-water scouring
FFBP	feed-forward back-propagation
FIS	fuzzy interference system
GA	genetic algorithm
GEP	gene expression programming
GP	grid partition
GT	Gamma test
IS	insertion sequence
LBS	live-bed scouring
LR	linear regression
MAPE	mean absolute percentage error
MFs	membership functions
MLP	multi-layer perceptron
MLR	multivariable linear regression
MSE	mean square error
R^2	coefficient of determination
RBF	radial basis function
RIS	root insertion sequence
RMSE	root mean square error
SDR	scour depth ratio

INTRODUCTION

Scouring around bridge piers is a result of the movement of bed sediment caused by the pier obstruction in the direction of flow (Kothyari *et al.* 1992). This obstruction leads to the acceleration of the flow, resulting in the formation of vertices around the pier that remove sediment from its vicinity. According to various research scholars (Ettema 1980; Melville & Coleman 2000; Kumar *et al.* 2012), the primary cause of sediment particle entrainment around bridge piers is the formation of vortices. The horseshoe vortex is not the cause of scouring, but rather a consequence of it and becomes effective in transporting material away from the scour hole (Breusers & Raudkivi 1991). The vortex formation is triggered by the flow in front of the pier separating from the bed and generating a scouring vortex due to the strong pressure field created by the pier. Wake vortices are predominant and act on the downstream side of the pier, causing accelerated side flow behind the pier and potentially resulting in a massive scour hole in the downstream side (Raudkivi & Ettema 1983). Due to the velocity gradient between the slower flow behind the pier and the faster flow on either side, a horseshoe vortex forms at the bottom of the upstream side, and a wake vortex forms on the downstream side, keeping sediment suspended. The flow field at a bridge pier is characterized by down-flow and surface rollers at the upstream side, horseshoe vortices at the bottom, and wake vortices on the downstream side, as indicated in Figure 1.

Many river bridges have collapsed because of heavy local scouring during high floods. Local scour depth refers to the erosion of dirt and rock particles located around the abutment or pier of a highway bridge that crosses over a water body to a certain depth. The scour depth is a significant factor in the bridge design as the base collapses due to improper scour depth estimation. Among two types of local scouring, clear-water scouring (CWS) is caused when the bed material upstream of the scour area is at rest and the shear stress of flow exceeds the critical shear stress, however, the live-bed scouring (LBS) takes place when there is general bed load movement and the upstream shear stress is greater than the threshold value. Laursen (1963) investigated the behavior of clear-water scours with geometry parameters, flow parameters, and sediment size and developed relationships for the scour in a long contraction, at an abutment, and around a pier. Ettema (1980) defined the influence of sediment size on scour depth at the circular shape of bridge piers for uniform sediments. Their experimental results showed that larger depths of clear-water scour can occur at piers placed in beds composed of uniform sediment armored by a layer of coarser sediment than that of the pier in a bed of uniform sediment. Raudkivi & Ettema (1983) reported that with smaller values of the flow depth to pier diameter ratio (y/b), the equilibrium scour depth reduces at a faster rate. They found that the decrease in the equilibrium depth is due to the interference of the water surface roller formed around the pier with the downward flow into the scour hole. Kothyari *et al.* (1992) proposed a semi-analytical method for predicting maximum scour depth at the bridge pier for LBS conditions. They considered the primary vortex in front of the pier to be the

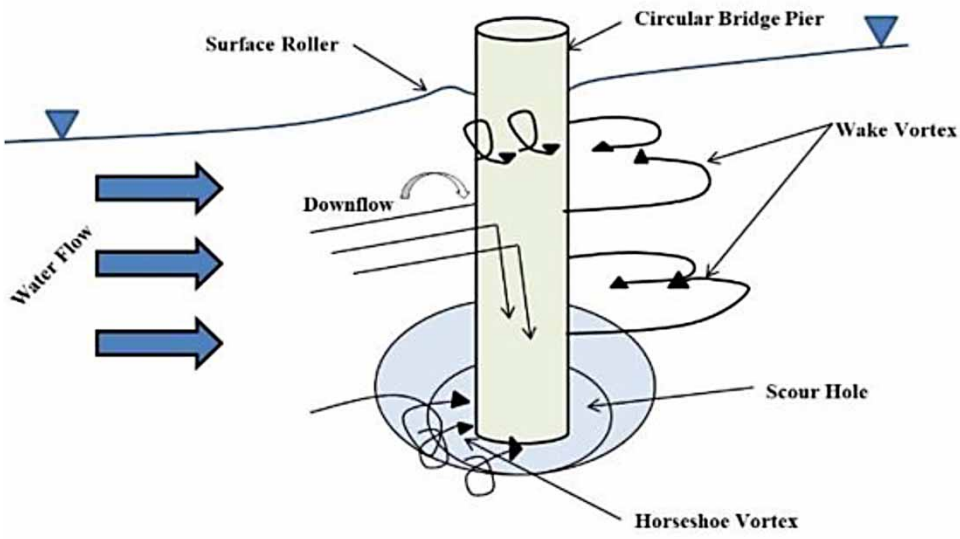

Figure 1 | Schematic diagram of local scour around a bridge pier.

prime agent causing scour at bridge piers. Sheppard *et al.* (2004) used a large-size model to explore clear-water local bridge pier scour and found that the concentration of suspended fine silt (wash load) has a major effect on equilibrium scouring depths through experiments. According to Raikar & Dey (2005), equilibrium scour depth increases as gravel size decreases and they found that the depth of scour in gravel beds is generally higher compared to the sand beds. Through experimentation, they found that the variation of equilibrium scour depth with gravel size represents a considerable deviation from the variation of this depth with sand size. Kothyari *et al.* (1992) proposed a scour depth model by considering actual and entrainment densiometric particle Froude numbers. They also developed a relationship for the temporal scour evolution at bridge foundation elements based on the similitude of Froude by relating the scour depth to the difference between the actual and the entrainment densiometric particle Froude numbers. From their experimental findings, Aksoy *et al.* (2017) reported that the scour depth was increased with pier diameter and flow velocity and developed a scour depth predictive model using flow velocity and the flow depth to pier diameter ratio (y/b). Pandey *et al.* (2018) reported the scour hole is created through the formation of an armor layer in a non-uniform gravel bed condition. Overall, the scour depth is significantly affected by the geometry of the pier, flow depth, approach flow velocity, and bed sediment size as it is evident from the lab and field experiments by different researchers. Hamidifar *et al.* (2021) investigated and verified different equations to determine the critical flow velocity ratio which was further used in estimating scour depth. They proposed better combinations of scour depth predictive model for CWS conditions.

Previously, many artificial intelligence (AI) techniques have been used for scour depth prediction, however, all these methods are not providing accurate results for different flow, geometry, and roughness conditions as well as for different types of scouring (Khan *et al.* 2012; Sharafati *et al.* 2021; Nil & Das 2023). The literature review of different AI techniques used in bridge pier scour depth modeling is presented in Table 1.

INFLUENCING PARAMETERS AND SCOUR DEPTH PREDICTION FORMULATIONS

The scour depth at a bridge pier is determined by the fluid flow, bed sediments, and pier characteristics.

Scour depth is described by the functional relationship:

$$d_s = f(\rho, \mu, U, U_c, g, y, d_{50}, \sigma, Fr, b) \tag{1}$$

where d_s is the scour depth, ρ is the fluid density, μ is the fluid dynamic viscosity, σ is the standard deviation of the bed sediment, g is the acceleration due to gravity, U is the approach mean velocity, U_c is the critical velocity, d_{50} is the median diameter of sediment, y is the flow depth, b is the pier diameter, Fr is the Froude number.

Table 1 | Previous studies on scour depth modeling using soft computing techniques

Authors	Input parameters and total number of datasets used	Soft computing technique used	Remarks
Bateni *et al.* (2007)	b, g, d_{50}, U, U_c, y, ρ, μ Laboratory data – 263	Artificial neural networks (ANN) – multi-layer perceptron (MLP), the radial basis function (RBF), and ANFIS	ANN-MLP had better performance in predicting equilibrium and the time-dependent scour depth around the bridge piers for CWS condition only
Firat (2009)	b, g, d_{50}, U, U_c, y, ρ, μ Laboratory data – 165	ANN – radial basis neural network (RBNN), ANFIS, and Multiple linear regression (MLR)	ANFIS model shows better performance in predicting scour depth. No mention about clear-water and LBS conditions
Firat & Gungor (2009)	b, g, d_{50}, U, U_c, y, ρ, μ Laboratory data – 165	Generalized Regression Neural Networks (GRNNs), Feed-Forward Neural Networks (FFNNs), and MLR	GRNN model had better performance for the selected data set. No mention about clear-water and LBS conditions
Kaya (2010)	b, h, K_{pn}, K_{pa}, Γ, V, y, d_{50}, Field data – 380	ANN	Model is developed for both clear-water and LBS conditions separately. ANN provide better results for the LBS data as compared to CWS dataset
Shin & Park (2010)	b, h, α^*, K_{pn}, g, V, y, ρ, μ Field data – 410	ANN-LMBP	ANN model provides better results as compared to HEC-18 and other empirical models. No mention about clear-water and LBS conditions
Muzzammil & Ayyub (2010)	b, Fr, y, σ_g Laboratory data – 130	ANN-Feed-Forward Back-Propagation (FFBP), Feed-Forward Cascade Correlation (FFCC), ANN-RBF, ANFIS and regression model	ANFIS model outperformed other and regression-based models for predicting scour depth. Pier diameter has a greater influence on equilibrium scour depth. No mention about clear-water and LBS conditions
Pal *et al.* (2011)	b, K_{pn}, K_{pa}, U, y, d_{50}, *and* σ_g Field data – 232	ANN-BPNN, ANN-GRNN, and radial basis function-based support vector regression (SVR-RBF)	SVR-RBF is the better scour depth predictor for their used dataset. Flow depth and the pier width are two important parameters affecting the scour depth prediction. No separate model for clear-water and LBS conditions
Toth & Brandimarte (2011)	b, K_{pa}, Ns^*, U, U_c, y, d_{50} Field data – 215; Laboratory data – 331	ANN-Newton Levenberg–Marquardt back-propagation algorithm (ANN-LM)	ANN models had the closest fit to measured scour depth in laboratory data under clear-water and LBS conditions and did not provide remarkable results for field data
Khan *et al.* (2012)	b, l, g, U, y, d_{50}, σ_g Laboratory data – 529	Gene expression programming (GEP) and ANN	GEP performs statistically slight inferior to ANN but significantly superior to other empirical models. No separate model for clear-water and LBS conditions
Etemad-Shahidi *et al.* (2015)	b, g, U, U_c, y, Fr, ρ, μ, d_{50} Laboratory data – 283	M5 model tree	Provide separate model for clear-water and LBS conditions
Sharafi *et al.* (2016)	b, l, g, U, y, r, n, d_{50}, σ_g, ρ_s Field data – 476	ANN, ANFIS, SVM, and nonlinear regression	SVM with polynomial kernel function provided better results. No mention about clear-water and LBS conditions
Khan *et al.* (2017)	b, U, y, d_{50} Laboratory data – total number is not available	ANN, genetic function (GF), and regression analysis	Genetic function-based model performed better than ANN and regression-based models for predicting clear-water scour depth only
Ebtehaj *et al.* (2017)	b, h, g, U, y, d_{50}, σ_g Laboratory data – 476	Self-adaptive extreme learning machine (SAELM), ANN, and SVM Particle swarm optimization (PSO)	SAELM performed better than other scour depth predictive models. No mention about clear-water and LBS conditions

(*Continued.*)

Table 1 | Continued

Authors	Input parameters and total number of datasets used	Soft computing technique used	Remarks
Shamshirband *et al.* (2020)	*b*, *l*, *Fr*, *U*, U_c, *y*, Re, d_{50}, and σ_g; Field data – 540 Laboratory data – 552		PSO provide better results compared to other scour depth model for their clear-water scour data set only. *b*/*y* and d_{50}/y were recognized as the most effective parameters for the laboratory and field data, respectively
Dang *et al.* (2021)	*b*, *g*, *U*, U_c, *y*, *Re*, d_{50} Laboratory data – 192	ANN-LM, ANN-PSO, ANN-FA (Firefly algorithm)	ANN-PSO is better in predicting the equilibrium scour depth as compared to ANN-LM and ANN-FA. Model is developed for CWS condition
Sreedhara *et al.* (2021)	d_{50}, sediment quantity, *U*, and flow time Laboratory data – total number is not available	Gradient tree boosting (GBT) and group method of data handling (GMDH)	GTB model performance was relatively superior to that of GMDH in the prediction of scour depth around different pier shapes and the model is developed for both CWS and LBS conditions
Nil & Das (2023)	*b*, *U*, U_c, *y*, Fr, d_{50} Laboratory data – 642	Support vector machine (SVM)	SVM with Gaussian and quadradic kernel function shows better results for CWS and LBS, respectively

b, pier diameter; *l*, pier length; g, acceleration due to gravity; *Fr*, Froude number; Re, Reynolds number; *h*, depth of collar below the free water surface; k_{pn}, pier nose shape factor; k_{pa}, pier alignment factor; *U*, flow velocity of the upstream from the pier, U_c, flow critical velocity; *w*, channel width, σ_g, standard deviation of grain size distribution; ϕ, dimensionless coefficient about the shape of the pier nose; α^*, opening ratio.

From the previous studies (Johnson 1995; Sheppard *et al.* 2004; Azmathullah *et al.* 2005; Nil & Das 2023), it is found that there are a group of dimensionless variables introduced to produce good results. The following relationship described maximum scour depth (d_{se}) in terms of dimensionless parameters:

$$\frac{d_{se}}{y} = f\left(\frac{b}{y}, \frac{d_{50}}{y}, \frac{U}{U_c}, \sigma, Fr\right) \tag{2}$$

In the absence of detailed information on the critical flow velocity (U_c), Neill's formula (Neill 1973) for the mean sediment size (d_{50}) particles can be used (Toth & Brandimarte 2011). So, this formula is also used here for calculating U_c as follows:

$$U_c = \varphi^{0.5} 31.08 y^{1/6} d_{50}^{1/3} \tag{3}$$

where y is the flow depth, and the Shields parameter, ϕ, in Equation (3) is computed with Equation (4), originally proposed by Miller *et al.* (1977) to relate the grain size to the shear velocity and then modified by Mueller (1996) for estimating the Shields parameter:

$$\begin{aligned} \varphi &= 0.0019 d_{50}^{-0.384} \quad \text{if } d_{50} < 0.0009\text{m} \\ \varphi &= 0.0942 d_{50}^{0.175} \quad \text{if } 0.0009\text{m} < d_{50} < 0.020\text{m} \\ \varphi &= 0.047 \quad \text{if } d_{50} > 0.020\text{m} \end{aligned} \tag{4}$$

The maximum scour depth to flow depth ratio was chosen as an output, and the five dimensionless parameters were chosen as inputs during the model development in this study. Different bridge pier scours depth predictive equations for clear-water and LBS are presented in Table 2, Equations (5)–(12).

In this paper, an attempt has been made to use two AI techniques such as adaptive network-based fuzzy inference system (ANFIS) and gene expression programming (GEP) in predicting the CWS depth ratio and LBS depth ratio (d_s/y), where d_s is scour depth and y is approach flow depth. Also, the most efficient model has been proposed for estimating local scour depth around the bridge pier.

METHODOLOGY

This section provides an in-depth discussion of the methods used in the present study to develop the ANFIS and GEP models for predicting scour depth. By reading this section, readers will gain a comprehensive understanding of the background and context of the model development process.

Gamma test

Agalbjorn *et al.* (1997) first documented the Gamma test, which was later developed and analyzed in depth by several analysts (Durrant 2001; Tsui *et al.* 2002; Das *et al.* 2020). The base mean square error (MSE) that contributes to input data selections is measured by gamma test (GT). The chosen input data can be used as part of a nonlinear model's structure. The logical purposes of intrigue can be found in Agalbjorn *et al.* (1997) and Noori *et al.* (2011). Another term is V-ratio, which restores a scaled invariant clamor evaluate in the vicinity of 0–1 and can be used to arrange the GT performance. The V-ratio can be described as:

$$V\text{-ratio} = \frac{\Gamma}{\sigma^2(y)} \tag{13}$$

where $\sigma^2(y)$ is the variance of yield 'y', which provides a standardized measure of the Gamma statistic and allows a judgment to be formed independent of the yield range on the issue of how effectively the yield can be depicted by a smooth function. The V-ratio is a useful statistic to consider when comparing yields or yields from different informational sets because it is independent of yield range. When the V-ratio is close to zero, then it indicates that the real yield is consistent (as measured by a smooth model). In the case where the V-ratio is close to one, then the yield is similar to the irregular commotion in terms of a smooth model. The GT may be achieved in practice by utilizing the winGamma program (Durrant 2001). This technology is

Table 2 | Different scour depth predictive equations used in the present study

Authors and years	Equation	Scouring condition	Eq. no.
Colemon (1972)	$\frac{d_s}{y} = 1.39(Fr)^{0.2}\left(\frac{b}{y}\right)^{0.9}$	LBS condition	5
Jain & Fischer (1979)	$\frac{d_s}{y} = 1.84\left(\frac{b}{y}\right)^{0.7} Fr_c^{0.25}$, for $Fr - Fr_c < 0$,	Both CWS and LBS conditions For $0 < \mathrm{Fr} - \mathrm{Fr_c} \leq 0.2$, the larger of the two scour depths computed from Equation (4) and (5) is used	6
	$\frac{d_s}{y} = 2\left(\frac{b}{y}\right)^{0.5}(Fr - Fr_c)^{0.25}$, for $Fr - Fr_c \geq 0.2$		7
Johnson (1995)	$\frac{d_s}{y} = 2.02\left(\frac{b}{y}\right)^{0.98} F_r^{0.21}\sigma^{-0.24}$	LBS condition	8
Ettema *et al.* (1998)	$\frac{d_s}{y} = \left(\frac{b}{y}\right)^{0.38}(Fr)^{0.2}\left(\frac{b}{d_{50}}\right)^{0.08}$	CWS condition	9
Yanmaz (2001)	$\frac{d_s}{b} = 1.564\left(\frac{y}{b}\right)^{0.405} F_r^{0.413}$	LBS condition	10
Kim *et al.* (2015)	$\frac{d_s}{y} = 0.69\left(\frac{b}{y}\right)^{0.35}\left(\frac{d_{50}}{y}\right)^{-0.10}\sigma^{0.39}Fr^{0.56}$	CWS condition	11
Sheppard *et al.* (2004)	$\frac{d_s}{y} = 2.5\left(\frac{b}{y}\right)f_1\left(\frac{y}{b}\right)f_2\left(\frac{U}{U_c}\right)f_3\left(\frac{b}{d_{50}}\right)$, where $f_1\left(\frac{y}{b}\right) = \tan h\left[\left(\frac{y}{b}\right)^{0.4}\right]$, $f_2\left(\frac{U}{U_c}\right) = 1 - 1.1.75\left[\ln\left(\frac{U}{U_c}\right)\right]^2$, and $f_3\left(\frac{b}{d_{50}}\right) = \left[\frac{\left(\frac{b}{d_{50}}\right)}{0.4\left(\frac{b}{d_{50}}\right)^{1.2} + 10.6\left(\frac{b}{d_{50}}\right)^{-0.13}}\right]$	CWS condition	12

quite successful and may be adopted for a variety of hydraulic nonlinear modeling. The *V*-ratio is a measure for assessing the predictability of the given yields based on readily available data. The dataset combination with a low mean square error (MSE) and *V*-ratio value is regarded as the most suitable input dataset for modeling.

Adaptive neuro-fuzzy inference system

The adaptive neuro-fuzzy inference system (neuro-FIS) uses a set of artificial neural networks (ANNs) and fuzzy systems to build fuzzy IF-THEN rules with suitable membership functions (MFs) obtained from the training pair, culminating in an inference. They eliminate the requirement for manual fuzzy system parameter optimization and instead rely on ANN to modify the system parameters. When ANN and FIS work together, they improve the system operation without requiring administrators to intervene.

Architecture and basic learning rules

ANFIS is a rule-based fuzzy rationale model whose rules are applied during the model's training process. This inference framework is built using five layers, as shown in Figure 2. In this network layout, the input (layer 0) and yield (layer 5) hubs reflect the input and yield origins, respectively. In the hidden layers, a few fixed and adjustable hubs serve as the MFs and rules. Two knowledge factors, x, and y have been considered, and a yield variable z is used to explain the methodology of the ANFIS model. If-then fuzzy rules are used in the ANFIS model to express the relationship between knowledge and yield and the model contains the two fuzzy rules that can be expressed as follows in terms of Takagi and Sugeno's form:

Rule 1: If x is A_1 and y is B_1 then $z_1 = p_1x + q_1y + r$

Rule 2: If x is A_2 and y is B_2 then $z_2 = p_2x + q_2y + r$

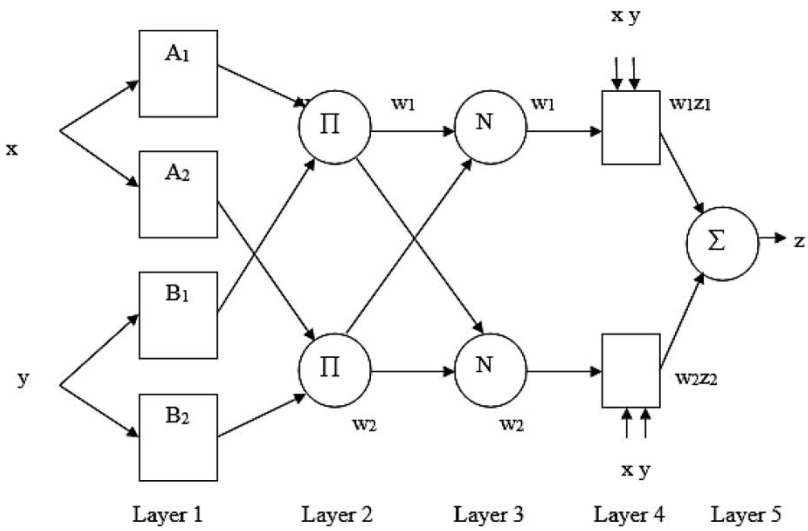

Figure 2 | A schematic diagram of the ANFIS structure.

The semantic levels are A_1, B_1, and A_2, B_2, and the ensuing parameters are p_1, q_1, r_1 and p_2, q_2, r_2. We have a zero-order TSK fuzzy-model if z_1 and z_2 are constants rather than linear equations. The ANFIS structure is comprised of five layers (Figure 2). The following are descriptions of the various layers: Layer 1 is the Fuzzification layer where every node is the flexible node with a node feature. Layer 2 is the Rule layer where every node is a fixed node that acts as the simple multiplier. Layer 3 is the Normalization layer and every node is an adaptive node with the letter N. The *i*th node determines the ratio of the terminating quality of the *i*th rule to the total of all terminating strengths. The fourth layer is the defuzzification layer and in this layer, every node has a purpose and is versatile. Layer 5 is the output layer, where a single node is a settled node that calculates the overall yield by adding all approaching signals.

The training procedure for this architecture aims to optimize two parameter settings so that ANFIS yield organizes the training data (Jang 1993). Figure 3 indicates the structure of the FIS. According to the ANFIS design, the overall yield '*z*' may be imparted as a linear mix of the outcome parameters given as the supplied values of the premise parameters. In light of this discovery, a hybrid learning standard is used to assess the feasibility of the precursor and succeeding parameters, which combines a back-propagation methodology with a least squares method (Jang 1991, 1993). The hybrid rule is defined in detail by Jang *et al.* (1997), who also claimed that it is significantly faster than the conventional back-propagation technique.

The number of input parameters is the primary constraint on the ANFIS model. If there are more than five ANFIS inputs, the computing time and rule numbers will increase, and ANFIS with grid partitioning will be unable to display yield. The general structure of the ANFIS forecasting system is shown in Figure 4.

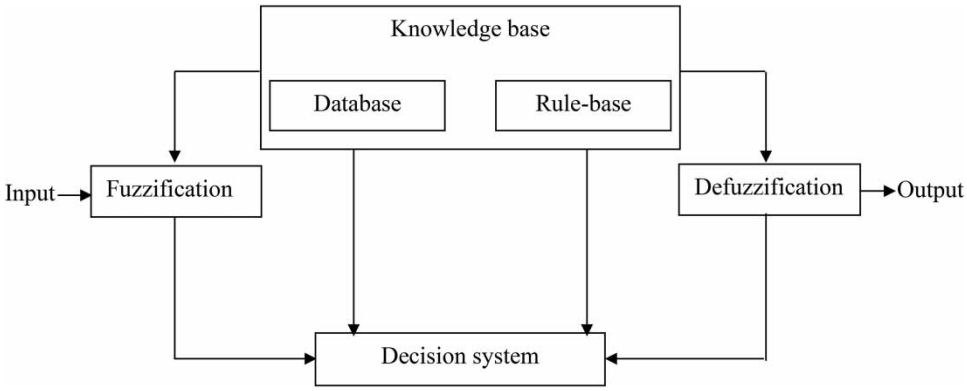

Figure 3 | General structure of the FIS.

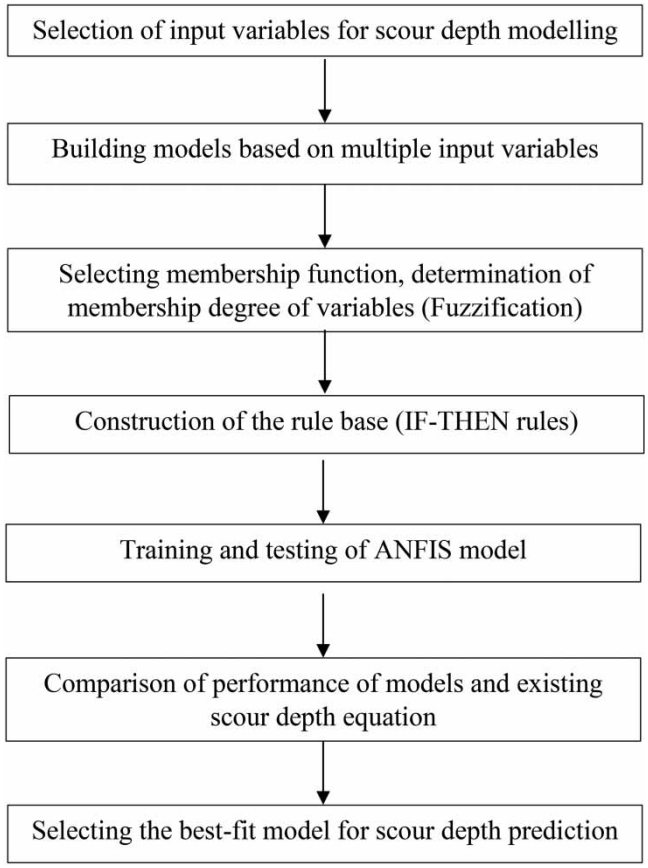

Figure 4 | General structure of the ANFIS forecasting system.

Grid partition

This methodology builds a Sugeno-type FIS structure from training datasets. Grid partition (GP) divides the input dataset into different neighboring fuzzy localities using a pivot-paralleled partition depending on a predetermined number of MFs. The eight types of MFs in the GP strategy are trimf, trapmf, gbellmf, gaussmf, gauss2mf, pmif, dsigmf, and psigmf. Each item of data can be expressed as a connection with the number of MFs (Muzzammil & Ayyub 2010). Only one yield can be used in a Sugeno-type. Either a linear or a constant yield function can be used for the selection of FIS type. This methodology generates the same number of rules as the number of yield MFs. The elective models in this subsection are made up of various FIS structures created using various MF features like (types and numbers) as the input MFs parameter.

Gene expression programming

GEP was created by Candida Ferreira in 1999 as a new evolutionary AI-based approach. This method is based on Koza's genetic programming (GP) methodology (1992). Similar to genetic algorithms (GAs), the genome is encoded as fixed-length linear chromosomes, which are subsequently represented as phenotypes by GEP in the form of expression trees. GEP combines the advantages of both of its predecessors, GA and GP, by avoiding some of their disadvantages. GEP is a full-featured genotype/phenotype approach that separates all elements. As a result, the fully functional genotype/phenotype system developed by GEP beats the conventional GP system (Ferreira 2002).

The mechanism in GEP, like other evolutionary approaches, begins with the random generation of the initial population. It consists of individual chromosomes of fixed length. One or more genes can be found on a chromosome. The fitness of each chromosome in the initial population is then calculated using a fitness function based on MSE. The fitness value of these chromosomes is then used to pick them by using the roulette wheel selection procedure. The better the chromosomes match; the more likely they are to be selected in the next generation. After selection, these are replicated with certain genetic operator modifications. Genetic operators such as mutation, inversion, transposition, and recombination are utilized to

change GEP. Mutation has been discovered to be the most powerful genetic operator and, in many circumstances, the only one available for chromosome modifications. The same modification approach is then applied to the new individuals, and the process is repeated until the maximum number of generations has been reached or the required precision has been obtained (Ferreira 2002). Several of these genetic operators used for chromosome genetic alteration are explained in the GEP scheme as follows (Ferreira 2006):

Mutation: Among all the operators, mutation is the most significant and powerful. In GEP modeling, mutations can occur anywhere in the genome. However, the structural composition of the chromosome should remain the same. In other words, the leading of a gene can replace the function with one of the other functions or ends, but only the end of the gene can be changed. When connected to the other terminal, the tail has no function. Thus, all the new individuals created by mutations are structurally correct programs.

Inversion: Inside the head of the gene, this operator inverts a sequence. It selects the chromosome, the gene to change, and the start and end points of the inverted head section.

Insertion sequence (IS) transposition: The IS elements are small parts of the genome with first-position function or termination. This operator randomly selects the chromosome or gene, as well as the beginning and end of the IS variable, and transposes them to the beginning of the gene immediately after the base.

Root insertion sequence (RIS) transposition: It is a small genomic fragment similar to the IS element, with the exception that starting point is always a function. It picks a chromosome, a gene to change, and starting and end points of the RIS element at random, and then transposes it to the gene's starting point.

Gene transposition: It occurs when the whole gene acts as transposing and transposes to the chromosome's beginning. Gene transposition differs from other types of transposition in that the transposon (gene) is deleted at the point of origin.

Single or double crossover/recombination: The parent chromosomes are coupled and the same spot is chosen in a single crossover. The gene is then swapped between the two chromosomes downstream of the crossover location. Two parent chromosomes are coupled in a double crossover, and two crossover locations are selected at random. The material that exists between the crossover locations is subsequently exchanged between parent chromosomes, resulting in the formation of two new offspring chromosomes (Guven & Aytek 2009).

Gene crossover: Gene fusion occurs when the whole genesis is swapped between the two parent chromosomes, resulting in the two offspring chromosomes with genes from both parents. Genes that are swapped are selected at random and located in the same location on parent chromosomes. Figure 5 shows an algorithm for gene expression programming (after Guven & Aytek 2009).

To create a predictive model for scour depth using AI techniques, it is crucial to establish input and output data sets for the ANFIS and GEP models to be trained and tested. These data sets have been sourced from published literature and will be further elaborated upon in the following section.

SOURCES OF DATASET

For the present study, many clear-water and LBS data have been taken from the literature and are presented in Tables 3 and 4 for circular/cylindrical bridge piers. The detailed data set are available in Supplementary file, Appendix A and Appendix B for CWS and LBS, respectively. Scour in the bridge depends on hydraulic parameters and sediment properties like pier diameter (b), flow depth (y), approach mean velocity (U), critical velocity (U_c), median diameter of sediment (d_{50}), Froude number (Fr) and geometric standard deviation of bed particle size (σ). In the present study, a total of 213 datasets for LBS modeling and 442 datasets are used for CWS modeling. The ranges of different parameters of CSW and LBS collected from the literature are depicted in Tables 3 and 4. Out of 213 LBS data, about 75% (159 sets) were selected for training and 25% (54 sets) were for testing. Table 3 shows the range of non-dimensional parameters used for clear-water scour modeling. Out of 442, about 75% (332 sets) were selected for training and 25% (110 sets) were selected for testing.

RESULTS AND DISCUSSION

Selection of best input parameter combination for modeling

In the present study, 50 different combinations of input parameters have been made in the winGamma software for clear-water and LBS separately. Out of 50, nine different combinations including the best input combinations are presented in Tables 5 and 6 for CWS and LBS, respectively. From Table 5, it is observed that the combination of the five parameters

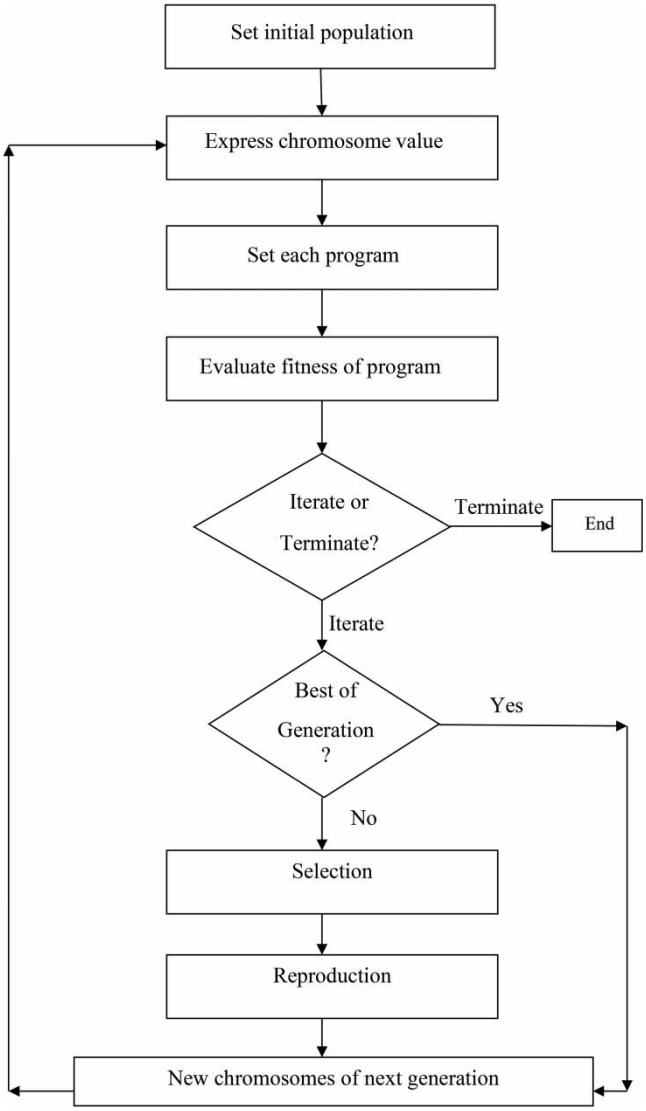

Figure 5 | Flow chart of GEP.

with mask [11111] can make a proper model for CWS as compared with other combinations due to its lesser values of Gamma and *V*-ratio which are very close to zero as compared to the other combination. From Table 6, it is observed that the combination of four parameters with mask [11011] shows the minimum Gamma and *V*-ratio values. In this blend, the U/U_c ratio is not included, however, this ratio is the most important parameter which influences the scour depth (Kothyari *et al.* 1992; Sheppard *et al.* 2004). The combination having five non-dimensional parameters is used for the ANFIS and GEP model development for clear-water and LBS.

Development of scour depth model using ANFIS

In this section, the scour depth of a bridge pier is modeled using the ANFIS approach is described. The input and yield data have been normalized to the domain [0.05, 0.95] using Equation (14) (Hsu *et al.* 2003) to get better accuracy of the model:

$$a_{\text{norm}} = 0.05 + 0.90\frac{(a - a_{\text{min}})}{(a_{\text{max}} - a_{\text{min}})} \tag{14}$$

where a_{norm} is the normalized input, a is the original input, a_{min} is the minimum of the input range, a_{max} is the maximum of the input range

Table 3 | Different parameters range for CWS collected from the literature

S. no	Author	b/y	d_{50}/y	U/U_c	σ	Fr
1	Chabert & Engeldinger (1956)	0.143–1.500	0.0007–0.0300	0.536–0.976	1.30	0.097–0.597
2	Shen *et al.* (1969)	0.713–1.299	0.0011–0.0020	0.533–0.882	1.40	0.103–0.213
3	Ettema (1976)	0.166–0.166	0.0009–0.0068	0.949–0.952	1.3–4.6	0.144–0.394
4	Jain & Fischer (1979)	0.498–0.994	0.0244–0.0244	0.808–1	1.30	0.499–0.618
5	Ettema (1980)	0.048–2.399	0.0003–0.1070	0.444–1	1.1–1.3	0.068–0.879
6	Chee (1982)	0.509–0.509	0.0038–0.0038	0.852–0.852	1.2–1.2	0.231–0.231
7	Chiew (1984)	0.151–0.265	0.0014–0.0152	0.795–0.977	1.2–4.3	0.170–0.480
8	Yanmaz & Altinbilek (1991)	0.285–1.486	0.0062–0.0237	0.447–0.737	1.1–1.3	0.230–0.234
9	Dey *et al.* (1995)	1.140–2.165	0.0052–0.0165	0.744–1	1.3–1.4	0.291–0.374
10	Graf (1995)	0.431–0.647	0.0090–0.0123	0.922–0.926	1.30	0.404–0.448
11	Melville (1997)	0.079–1.665	0.0039–0.0075	0.438–0.820	1.30	0.124–0.267
12	Melville & Chiew (1999)	0.190–1.000	0.0048–0.0136	0.415–0.904	1.30	0.122–0.382
13	Sheppard *et al.* (2004)	0.090–1.634	0.0001–0.0052	0.689–0.909	1.2–1.5	0.072–0.276
14	Sheppard & Miller (2006)	0.310–0.362	0.0005–0.0019	0.560–0.870	1.30	0.084–0.180
15	Ettema *et al.* (2006)	0.064–0.406	0.0010–0.0010	0.858–0.858	1.30	0.147–0.147
16	Pandey *et al.* (2018)	0.400–1.459	0.0024–0.1259	0.220–0.970	1.12–1.23	0.220–0.970
17	Pandey *et al.* (2020a)	0.471–1.350	0.0250–0.0856	0.708–0.984	1.51–1.88	0.433–0.713
18	Pandey *et al.* (2020b)	0.550–1.350	0.0395–0.0474	0.660–0.940	1.38–1.38	0.424–0.553

Table 4 | Different parameters range for LBS collected from the literature

S. no	Author	b/y	d_{50}/y	U/U_c	σ	Fr
1	Chabert & Engeldinger (1956)	0.214–1	0.0015–0.0052	1.029–1.309	1.30	0.189–0.378
2	Shen *et al.* (1969)	0.568–1.500	0.0006–0.0026	1.033–3.941	1.4–2.2	0.198–0.951
3	Jain & Fischer (1979)	0.206–0.994	0.0024–0.0244	1.025–4.690	1.30	0.499–1.498
4	Chee (1982)	0.509–1.021	0.0024–0.0140	1.114–4.298	1.2–1.3	0.302–1.213
5	Chiew (1984)	0.085–0.412	0.0013–0.0152	1.007–3.101	1.2–5.5	0.178–0.881
6	Sheppard *et al.* (2004)	0.250–1.668	0.0001–0.0012	1.088–1.190	1.5–1.5	0.115–0.223
7	Sheppard & Miller (2006)	0.355–0.757	0.0006–0.0028	1.386–5.360	1.30	0.299–1.260

Table 5 | Selection of the best combination for CWS

Experiment no.	Combination of input parameters	Gamma	Std. error	*V*-ratio	Mask
1	**All input**	**0.013**	**0.0026**	**0.054**	**11111**
2	All input – d_{50}/y	0.015	0.0029	0.059	10111
3	All input – σ	0.021	0.0043	0.083	11101
4	All input – Fr	0.015	0.0031	0.062	11110
5	All input – d_{50}/y, σ	0.031	0.0067	0.126	10101
6	All input – d_{50}/y, σ, Fr	0.059	0.0056	0.236	10100
7	All input – U/U_c	0.018	0.0030	0.073	11011
8	All input – U/U_c, σ	0.021	0.0029	0.085	11001
9	All input – U/U_c, Fr	0.037	0.0040	0.147	11010

Table 6 | Selection of the best combination for LBS

Experiment no.	Combination of input parameters	Gamma	Std. error	*V*-ratio	Mask
1	**All input**	**0.024**	**0.0036**	**0.098**	**11111**
2	All input – d_{50}/y	0.024	0.0021	0.095	10111
3	All input – σ	0.024	0.0029	0.096	11101
4	All input – Fr	0.027	0.0037	0.108	11110
5	All input – d_{50}/y, σ	0.024	0.0039	0.098	10101
6	All input – d_{50}/y, σ, Fr	0.039	0.0034	0.156	10100
7	***All input – U/U_c***	***0.022***	***0.0032***	***0.087***	***11011***
8	All input – U/U_c, σ	0.024	0.0033	0.095	11001
9	All input – U/U_c, Fr	0.052	0.0106	0.206	11010

Note: Bold values indicate the best model output.

Performance of ANFIS model for CWS

To check the performance of the present model different statistical error indices like mean absolute percentage error (MAPE) and coefficient of determination (R^2) are utilized as mentioned in Khuntia *et al.* (2019), Das *et al.* (2020), Devi *et al.* (2021) and Kumar *et al.* (2023). In Table 7, there are 16 combinations made with different MFs and different MF types for CWS using normalized data. Out of 16 combinations, the membership function [22222] and MF type (gbellmf) of the fifth number combination shows $R^2 = 0.95$ which is better than other combinations. The performance of various models of clear-water is presented in Table 7.

Performance of ANFIS model for LBS

In Table 8, there are 16 combinations made with different MFs and different membership function types for LBS using normalized data. Out of 16 combinations, the membership function [33222] and MF type (gaussmf) of the tenth number

Table 7 | Performance of various ANFIS models of CWS using normalized data

			Training		Testing		Total dataset	
Serial No.	Membership function	MF type	R^2	MAPE	R^2	MAPE	R^2	MAPE
1	22222	trapmf	0.97	10.246	0.87	16.595	0.95	11.823
2	33222	trapmf	0.98	9.103	0.53	24.533	0.86	12.943
3	33322	trapmf	0.98	8.031	0.25	32.364	0.74	14.162
4	33333	trapmf	0.98	7.110	0.55	24.929	0.87	11.544
5	**22222**	**gbellmf**	**0.99**	**6.961**	**0.86**	**16.718**	**0.95**	**9.395**
6	33222	gbellmf	0.99	5.202	0.46	22.083	0.84	9.403
7	33322	gbellmf	0.99	3.621	0.47	30.407	0.83	10.288
8	33333	gbellmf	0.99	2.525	0.63	23.117	0.91	7.673
9	22222	gaussmf	0.99	6.927	0.79	20.017	0.94	10.185
10	33222	gaussmf	0.99	5.572	0.70	21.774	0.92	9.622
11	33322	gaussmf	0.99	4.630	0.73	23.728	0.93	9.405
12	33333	gaussmf	0.99	3.939	0.37	43.416	0.77	13.764
13	22222	gauss2mf	0.98	8.974	0.50	40.079	0.80	16.715
14	33222	gauss2mf	0.99	6.333	0.61	19.160	0.89	9.526
15	33322	gauss2mf	0.99	4.922	0.51	22.856	0.75	9.385
16	33333	gauss2mf	0.99	4.356	0.33	42.769	0.74	13.88

Note: Bold values indicate the best model output.

Table 8 | Performance of various ANFIS models of LBS using normalized data

Serial no.	Membership function	MF type	Training		Testing		Total dataset	
			R^2	MAPE	R^2	MAPE	R^2	MAPE
1	22222	trapmf	0.98	5.439	0.80	13.819	0.93	7.564
2	33222	trapmf	0.99	3.879	0.82	14.017	0.94	6.450
3	33322	trapmf	0.99	3.025	0.66	25.436	0.90	8.707
4	33333	trapmf	0.99	2.269	0.59	22.980	0.86	7.520
5	22222	gbellmf	0.99	3.665	0.28	31.826	0.47	10.605
6	33222	gbellmf	0.99	1.340	0.31	24.369	0.64	7.178
7	33322	gbellmf	0.99	0.800	0.50	23.566	0.82	6.571
8	33333	gbellmf	0.99	0.294	0.69	18.741	0.91	4.903
9	22222	gaussmf	0.99	3.918	0.60	15.288	0.84	6.801
10	**33222**	**gaussmf**	**0.99**	**2.776**	**0.81**	**12.697**	**0.95**	**5.291**
11	33322	gaussmf	0.99	1.421	0.41	23.110	0.76	6.920
12	33333	gaussmf	0.99	0.356	0.75	14.347	0.93	3.906
13	22222	gauss2mf	0.99	4.302	0.81	13.727	0.94	6.691
14	33222	gauss2mf	0.99	2.817	0.70	45.011	0.91	5.910
15	33322	gauss2mf	0.99	1.969	0.46	26.170	0.78	8.105
16	33333	gauss2mf	0.99	1.157	0.72	19.587	0.91	5.830

Note: Bold values indicate the best model output.

combination shows $R^2 = 0.95$ which is better than other combinations. The performance of various models of CWS is presented in Table 8.

Development of scour depth model using GEP

In this section, the scour depth of a bridge pier is modeled using the GEP approach is described. The GEP model is developed for the prediction of the scour depth by incorporating five independent input parameters. GeneXpro Tools 5.0 software package is used for the present study.

GEP model for CWS

Table 9 shows the performance of the GEP model for CWS using normalized data. Using these data, four attempts have been done with the variation of chromosome number, fitness function, and number of runs for modeling the CWS and LBS. Table 9 demonstrates the performance of the GEP model for CWS using normalized data and Table 10 shows the corresponding parameters of the optimized GEP model. In Table 9, the coefficient of determination (R^2) and MAPE values are depicted for the training and testing stage. Here, trial number 2 has been selected as less error is found in terms of R^2 and MAPE.

Table 9 | Performance of the GEP model for CWS using normalized data

Trial No.	Chro-somes	Fitness function	No. of runs	Training		Testing		Total dataset	
				R^2	MAPE	R^2	MAPE	R^2	MAPE
1	30	MSE	65,000	0.817	25.817	0.805	26.764	0.808	26.053
2	**30**	**MSE**	**100,000**	**0.885**	**20.346**	**0.855**	**24.468**	**0.880**	**21.372**
3	30	RMSE	100,000	0.861	23.938	0.716	30.999	0.827	25.695
4	50	MSE	55,000	0.844	24.483	0.821	26.987	0.835	25.106

Note: Bold values indicate the best model output.

Table 10 | Parameters of the optimized GEP model for CWS modeling

Serial no.	Description of parameter	Parameters setting
1	Chromosomes	30
2	Genes	3
3	Head size	8
4	Number of generations	100,000
5	Mutation rate	0.044
6	Inversion rate	0.1
7	Function set	(+, -, *, /, Pow, Exp, In)
8	Crossover frequency	0.5
9	One point recombination rate	0.3
10	Two-point recombination rate	0.3
11	Gene recombination rate	0.1
12	Gene transposition rate	0.1
13	Linking function	Addition
14	Program size	26
15	Fitness function	MSE

The expression tree for CWS is presented in Figure 6. In this expression tree $d_0 = b/y$, $d_1 = d_{50}/y$, $d_2 = U/U_c$, $d_3 = \sigma$, $d_4 = Fr$. In Sub-ET 1, C8 is a constant and the value is 6.27. The equation of this expression tree is expressed in Equation (15).

The equation obtained from the sub-ETs to form the GEP model for CWS may be expressed as:

$$\frac{d_s}{y} = \left[6.27 \times \left\{\left(\ln\left(\frac{U}{U_c}\right) \times \frac{b}{y}\right) \times \left(\frac{b}{y} \times \sigma\right)\right\}\right] + \left[Fr - \frac{d_{50}}{y}\right] + \left[\frac{b}{y} - \left\{\left((\sigma)^{\frac{b}{y} \times \frac{1}{Fr}}\right) \times \left(\left(Fr - \frac{d_{50}}{y}\right) + \left(\frac{b}{y}\right)\right)\right\}\right] \tag{15}$$

GEP model for LBS

Table 11 depicts the performance of the GEP model for LBS using normalized data and Table 12 shows the parameters of the optimized GEP model for LBS. The results are presented in Table 11 for LBS. In Table 11, trial number 1 shows a low MAPE value and high R^2 value but the expression tree of trial number 1 is complex. In trial number 2, the R^2 and MAPE values are more than the trial number, however, it has been selected for the present study as the expression tree of trial number 2 is not very complex as compared to the expression of trial no 1.

The scour depth formula is shown in the form of an expression tree for the live-bed in Figure 7. In this expression tree $d_0 = b/y$, $d_1 = d_{50}/y$, $d_2 = U/U_c$, $d_3 = \sigma$, $d_4 = Fr$. In Sub-ET 1 C5, Sub-ET 3 C5, Sub-ET 3 C8 is constant and the value of C5 = −0.1, C5 = −0.1 and C8 = 7.92. The equation of this expression tree is expressed in Equation (16).

The equation obtained from the GEP model for LBS may be expressed as:

$$\frac{d_s}{y} = \left[\frac{b}{y} + \left\{\left(\ln\left(\frac{d_{50}}{y}\right) \times \left(Fr - \frac{b}{y}\right)\right) \times \left(\left(\frac{b}{y} - Fr\right) \times (-0.1)\right)\right\}\right] + Fr + \left[-0.1\left\{\left(\left(\sigma + \frac{b}{y}\right) - \left(\frac{U}{U_C}\right)\right) + ((7.92 - Fr) \times (Fr))\right\}\right] \tag{16}$$

$$\frac{d_s}{y} = \left[\frac{b/y}{\{(-3.888 + \sigma) + (\sigma/Fr)\} - \{(b/y)^{-1.584} + (d_{50}/y)\}}\right] + \left[\frac{Fr}{\{(e)^{\sigma}/((e)^{b/y})^{U/U_C}\}}\right] + \left[\frac{b}{y} - \left\{\frac{Fr}{\frac{e^{(U/U_c - (-3.519))}}{Fr/(b/y)}}\right\}\right] \tag{17}$$

Scour depth ratio (SDR) ($=d_s/y$) value computed using Equation (17) gives a MAPE value of 12.9% but using Equation (16), it is found to be 14.2% for the testing case and 15.30% for the total dataset (Table 11). However, the expression of Equation

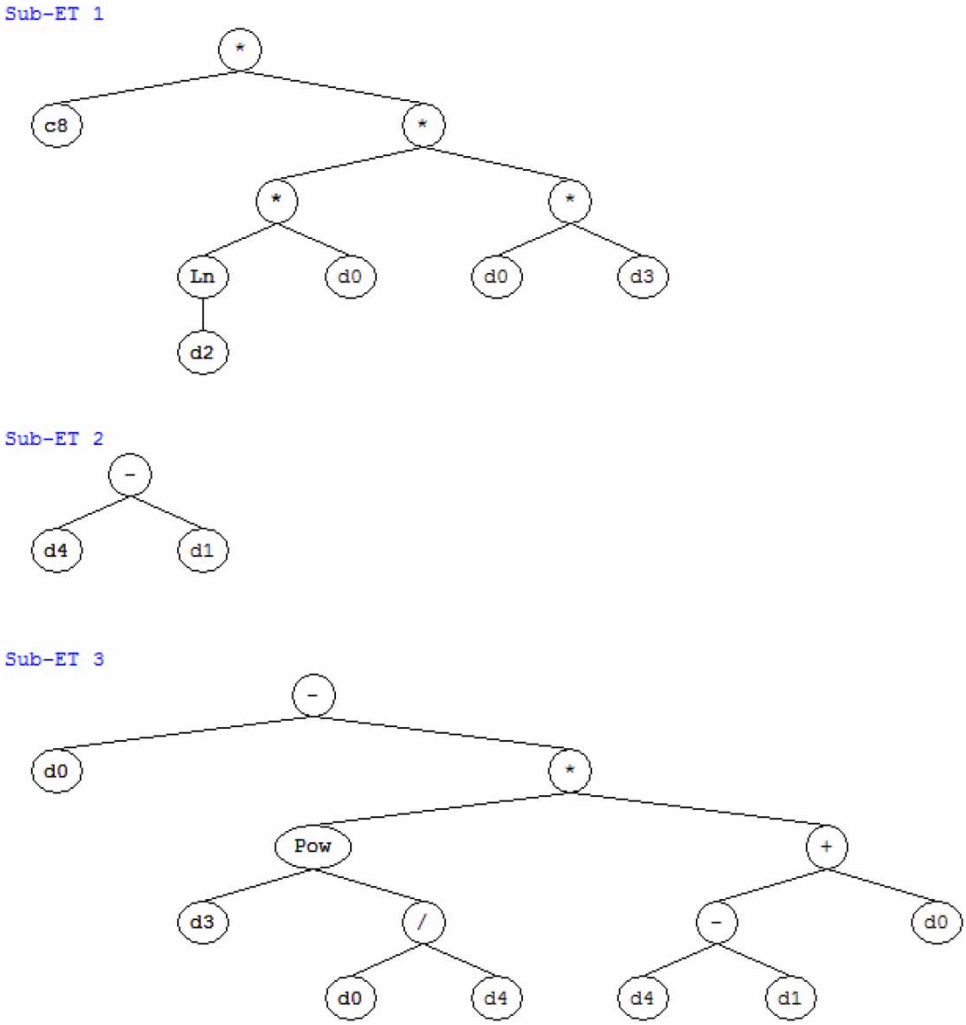

Figure 6 | Expression tree for CWS.

(16) is simpler than Equation (17) as it contains one logarithmic operator only. Therefore, for this present research, Equation (16) is suggested to be used in predicting the d_s/y value for LBS conditions.

For CWS condition, the result shows (see Tables 7 and 9) that the ANFIS model provides an R^2 value of 0.95 and MAPE value of 9.39% and corresponding values for GEP model are 0.88 and 21.37%. For LBS the result shows (see Tables 8 and 10) ANFIS model provides an R^2 value of 0.95 and MAPE value of 5.29% and corresponding values for GEP model are 0.90 and 15.31%. Thus, it has been found that the proposed ANFIS model is providing better results than the present GEP model. Comparison plots of observed and predicted SDR by different scour depth models for CWS and LBS are shown in Figures 8 and 9 respectively. In Figure 8, the SDR values obtained from the developed ANFIS lie very close to the best-fit line (45° line i.e., line of good agreement) as compared to the developed GEP model and other scour depth predictive models (Jain & Fischer 1979; Ettema *et al.* 1998; Sheppard *et al.* 2004; Kim *et al.* 2015) for CWS condition. The SDR value obtained from Jain & Fischer (1979) and Sheppard *et al.* (2004) models lie above the best-fit line indicating the overestimation of SDR values. It is observed in Figure 8 that for observed SDR < 1.0, Ettema *et al.*'s (1998) scour depth model is overestimating the SDR and for observed SDR > 1.0, it is underestimating. For observed SDR > 0.80, the Kim *et al.* (2015) clear-scour depth predictive model results lie below the best-fit line indicating an underestimation of the SDR.

In Figure 9, the SDR values obtained from the developed ANFIS and GEP lie very close to the best-fit line as compared to other scour depth predictive models (such as Colemon 1971; Jain & Fischer 1979, Johnson 1995; Yanmaz 2001) for LBS condition. The predicted SDR values from all the models are found to be very close to the best-fit line, for low observed values

Table 11 | Performance of the GEP model for LBS using normalized data

				Training		Testing		Total dataset	
Trial No.	Chromosomes	Fitness function	No. of runs	R^2	MAPE	R^2	MAPE	R^2	MAPE
1	30	MSE	65,000	0.923	15.235	0.875	12.954	0.911	14.657
2	**30**	**MSE**	**100,000**	**0.910**	**15.685**	**0.870**	**14.204**	**0.900**	**15.310**
3	30	RMSE	100,000	0.915	15.991	0.871	14.772	0.904	15.682
4	50	MSE	55,000	0.922	16.697	0.863	14.647	0.910	16.178

Note: Bold values indicate the best model output.

Table 12 | Parameters of the optimized GEP model for LBS modeling

Serial no.	Description of parameter	Parameter setting
1	Chromosomes	30
2	Genes	3
3	Head size	8
4	Number of generations	125,000
5	Mutation rate	0.044
6	Inversion rate	0.1
7	Function set	(+, −, *, /, Pow, Exp, ln)
8	Crossover frequency	0.5
9	One point recombination rate	0.3
10	Two-point recombination rate	0.3
11	Gene recombination rate	0.1
12	Gene transposition rate	0.1
13	Linking function	Addition
14	Program size	28
15	Fitness function	MSE

(i.e., 0.4–0.6) except for Jain & Fischer's (1979) scour depth predictive model. For the LBS data set used in the present research, it is found that the values predicted from the Jain & Fischer (1979) and Johnson (1995) models are higher than most of the observed SDR values and for Colemon (1972) model, it is lower than the observed values.

Statistical error analysis

The statistical error indices such as MAPE, root mean square error (RMSE), and coefficient of determination (R^2) are computed for both the present models i.e., ANFIS and GEP models along with four scour depth predictive equations such as Jain & Fischer (1979), Ettema *et al.* (1998), Sheppard *et al.* (2004), Kim *et al.* (2015), and was compared to different conditions. By examining the error for different ranges of b/y, U/U_c, and Fr, it is possible to determine the strength of present models and other existing equations, which are most useful under various conditions.

In CWS, the following ranges are selected for b/y, U/U_c, and Fr:

(a) $b/y < 0.25$, $0.25 \leq b/y < 0.5$, $0.5 \leq b/y < 1.0$, $1 \leq b/y < 1.5$ and $b/y \geq 1.5$
(b) $U/U_c < 0.5$, $0.5 \leq U/U_c < 0.7$, $0.7 \leq U/U_c < 0.8$, $0.8 \leq U/U_c < 0.9$, and $0.9 \leq U/U_c < 1.0$
(c) $Fr < 0.20$, $0.20 \leq Fr < 0.40$, $0.40 \leq Fr < 0.6$, $0.60 \leq b/y < 0.80$, and $0.8 \leq Fr < 1.0$

In LBS, the following ranges are selected for b/y, U/U_c, and Fr:

(a) $b/y < 0.25$, $0.25 \leq b/y < 0.5$, $0.5 \leq b/y < 1.0$, and $1.0 \leq b/y < 1.5$
(b) $1.0 < U/U_c < 1.2$, $1.2 \leq U/U_c < 1.5$, $1.5 \leq U/U_c < 2.5$, $2.5 \leq U/U_c < 3.5$ and $U/U_c \geq 3.5$

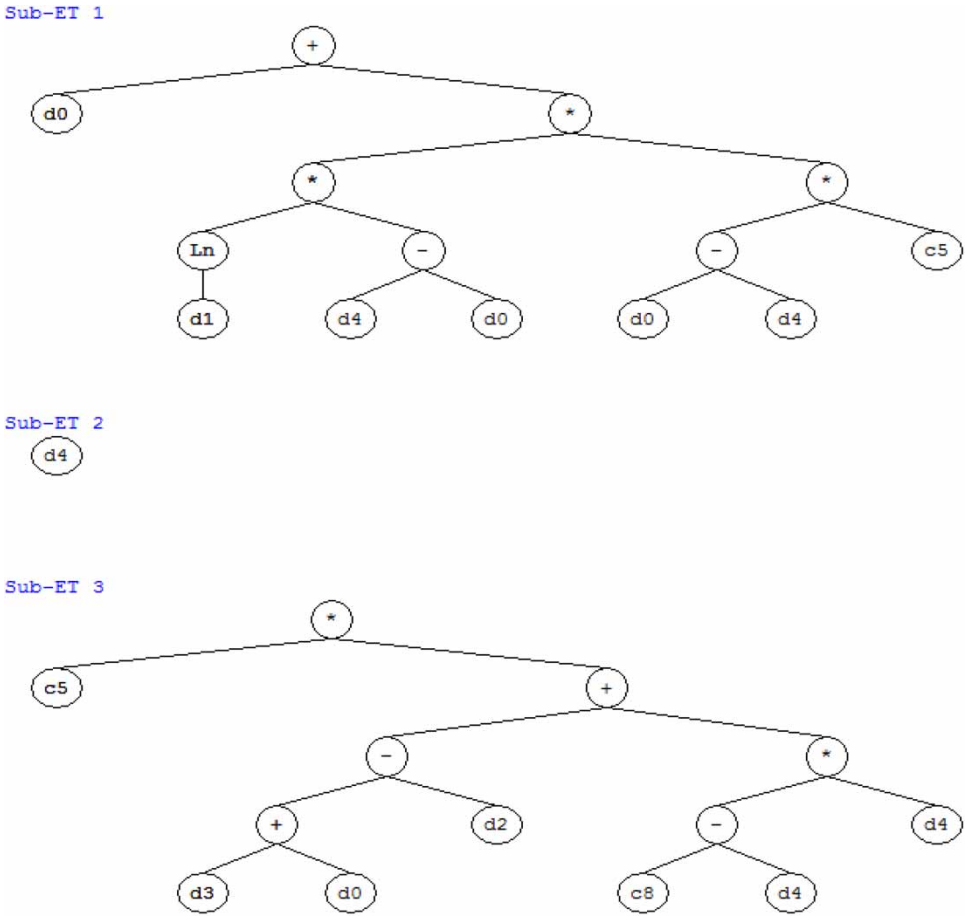

Figure 7 | Expression tree for LBS.

(c) $Fr < 0.25$, $0.25 \leq Fr < 0.50$, $0.50 \leq Fr < 0.75$, $0.75 \leq b/y < 1.0$, and $Fr \geq 1.0$

Table 13(a)–13(c) provides the MAPE, RMSE, and R^2 values of two present models and four scour depth predictive equations for selected ranges of b/y, U/U_c, and Fr, respectively. For $b/y < 0.25$, MAPE is high for Ettema *et al.* (1998), Kim *et al.* (2015), GEP (present model), and Sheppard *et al.* (2004). In addition, RMSE is high for Jain & Fischer (1979), GEP (present model), Kim *et al.* (2015) and Ettema *et al.* (1998) and R^2 is low for Kim *et al.* (2015) and Jain & Fischer (1979). For both $0.5 \leq b/y < 1.0$ and $1.0 \leq b/y < 1.5$, MAPE and RMSE are high for Sheppard *et al.* (2004), Kim *et al.* (2015), Ettema *et al.* (1998) and Jain & Fischer (1979). For $b/y \geq 1.5$, MAPE is high for Jain & Fischer (1979), Sheppard *et al.* (2004), and Kim *et al.* (2015). In addition, RMSE is high for Sheppard *et al.* (2004), Kim *et al.* (2015) and Ettema *et al.* (1998) and R^2 is low for GEP, Kim *et al.* (2015) and Ettema *et al.* (1998). At all the ranges of b/y, ANFIS (present model) performs well with minimum MAPE and RMSE and high R^2 value. Table 13(b) provides the MAPE, RMSE, and R^2 values for two present models and four scour depth predictive equations for selected ranges of U/U_c. For $U/U_c < 0.5$, MAPE is high for all the approaches. In addition, RMSE is high for Sheppard *et al.* (2004), Jain & Fischer (1979), GEP (present model), Kim *et al.* (2015), and Ettema *et al.* (1998), and R^2 is low for Kim *et al.* (2015), Jain & Fischer (1979), however, the ANFIS model provides R^2 value close to 0.90. For both $0.5 \leq U/U_c < 0.7$ and $0.7 \leq U/U_c < 0.8$, Jain & Fischer (1979), Ettema *et al.* (1998), Sheppard *et al.* (2004) and Kim *et al.* (2015) show R^2 value in the range of 0.44–0.68. MAPE and RMSE are high for Ettema *et al.* (1998). For $0.8 \leq U/U_c < 0.9$, Jain & Fischer (1979) and Ettema *et al.* (1998) shows a very high MAPE which considers the (b/d_{50}) value in their equation. Sheppard *et al.* (2004) show an R^2 value greater than 0.70 with an RMSE value of 0.52 for $0.9 \leq U/U_c < 1.0$. The developed ANFIS model provides MAPE of less than 15% and an R^2 value of more than 0.90 for all ranges except $U/U_c < 0.5$. In Table 13(c), for $Fr < 0.2$, the least MAPE and

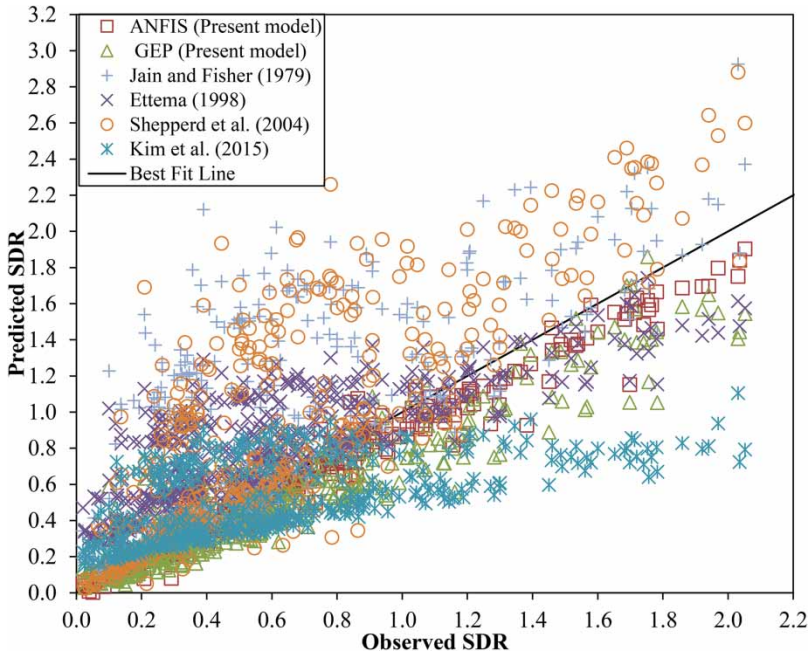

Figure 8 | Comparison of observed vs. predicted SDR by different scour depth models for CWS.

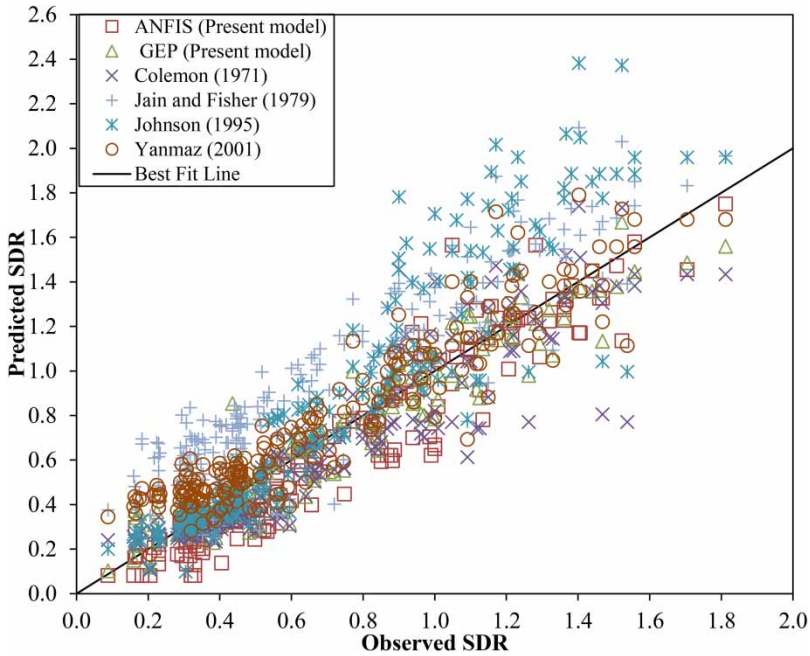

Figure 9 | Comparison of observed vs. predicted SDR by different scour depth models for LBS.

RMSE are found from the ANFIS model with a high R^2 value. Further, the errors are gradually reduced for high values of *Fr*. However, the previous models are providing unsatisfactory results with high errors and low R^2 values.

Table 14(a)–14(c) provides the MAPE, RMSE, and R^2 values found from the present approaches and four scour depth predictive equations, for selected ranges of b/y, U/U_c, and *Fr*, respectively. In Table 14(a), it is observed that the Johnson (1995) model renders less values of MAPE for the low range of b/y (<0.25), and present approaches failed to provide satisfactory

Table 13 | (a) Error analysis of different approaches in estimating *ds/y* in the CWS condition and selected ranges of *b/y*

Different approaches	$b/y < 0.25$	$0.25 \le b/y < 0.5$	$0.5 \le b/y < 1.0$	$1 \le b/y < 1.5$	$b/y \ge 1.5$
ANFIS (Present model)	23.22 0.06 0.87	11.25 0.08 0.88	12.81 0.12 0.93	12.11 0.18 0.89	10.81 0.25 0.67
GEP (Present model)	45.92 0.11 0.74	27.71 0.19 0.67	30.17 0.22 0.76	21.46 0.24 0.79	14.29 0.31 0.30
Jain & Fischer (1979)	25.44 0.46 0.24	109.11 0.84 0.01	151.98 0.66 0.02	38.10 0.18 0.46	88.22 0.11 0.68
Ettema *et al.* (1998)	192.19 0.24 0.69	58.05 0.25 0.40	109.46 0.45 0.29	54.61 0.42 0.38	15.40 0.32 0.16
Sheppard *et al.* (2004)	42.46 0.09 0.71	43.76 0.39 0.16	121.76 0.80 0.05	107.64 0.84 0.11	34.12 0.59 0.48
Kim *et al.* (2015)	93.55 0.13 0.33	38.67 0.24 0.16	74.40 0.40 0.02	43.26 0.50 0.03	52.88 0.95 0.30

Note: Three values presented in each cell represent MAPE, RMSE, and R^2, respectively.

Table 13 | (b) Error analysis of different approaches in estimating *ds/y* in the CWS condition and selected ranges of U/U_c

Different approaches	$U/U_c < 0.5$	$0.5 \le U/U_c < 0.7$	$0.7 \le U/U_c < 0.8$	$0.8 \le U/U_c < 0.9$	$0.9 \le U/U_c < 1.0$
ANFIS (Present model)	48.55 0.12 0.89	13.84 0.10 0.93	14.57 0.15 0.95	14.12 0.10 0.98	13.38 0.12 0.95
GEP (Present model)	94.39 0.19 0.70	35.10 0.20 0.74	36.46 0.27 0.87	26.98 0.18 0.91	25.38 0.15 0.92
Jain & Fischer (1979)	323.44 0.44 0.57	38.31 0.36 0.53	69.82 0.45 0.60	90.30 0.54 0.54	109.07 0.56 0.54
Ettema *et al.* (1998)	272.29 0.36 0.59	46.18 0.24 0.62	74.24 0.33 0.68	104.72 0.37 0.67	113.46 0.38 0.66
Sheppard *et al.* (2004)	271.58 1.72 0.50	39.06 0.21 0.53	46.82 0.37 0.66	67.17 0.49 0.75	87.25 0.52 0.74
Kim *et al.* (2015)	121.64 0.22 0.68	37.54 0.31 0.52	55.78 0.49 0.44	61.01 0.38 0.37	74.46 0.35 0.36

Note: Three values presented in each cell represent MAPE, RMSE, and R^2, respectively.

results, due to fewer numbers of input data sets in this range. For $b/y > 1.5$, it has been observed that the present ANFIS model shows an R^2 value of 0.67 indicating the poor performance of the model in this domain as there are only 12 input data sets in the training and testing stage. However, the present GEP model shows less error and high R^2 values for all other ranges of *b/y* value. Table 14(b) demonstrates that the present GEP model and Colemon (1972) render less values of MAPE and RMSE for all the ranges of U/U_c. However, the present GEP model shows the least error for all the ranges of U/U_c value. In Table 14(c), it is observed from the error analysis that for $Fr < 0.25$, the present GEP model and

Table 13 | (c) Error analysis of different approaches in estimating *ds/y* in the CWS condition and selected ranges of Fr

Different approaches	$Fr < 0.20$	$0.20 \leq Fr < 0.40$	$0.40 \leq Fr < 0.6$	$0.60 \leq b/y < 0.80$	$0.8 \leq Fr < 1.0$
Present model (ANFIS)	20.07	12.99	15.81	10.92	11.20
	0.07	0.13	0.11	0.13	0.22
	0.90	0.95	0.96	0.88	0.92
Present model (GEP)	44.67	28.54	33.20	18.03	30.52
	0.13	0.24	0.19	0.13	0.23
	0.68	0.88	0.87	0.89	0.90
Jain & Fischer (1979)	92.16	33.10	135.28	212.72	281.00
	0.18	0.25	0.61	0.91	1.18
	0.47	0.83	0.49	0.63	0.70
Ettema *et al.* (1998)	183.69	47.25	123.26	133.19	158.01
	0.30	0.23	0.41	0.53	0.63
	0.57	0.84	0.54	0.70	0.76
Sheppard *et al.* (2004)	53.38	43.92	114.94	145.54	146.67
	0.12	0.69	0.67	0.71	0.71
	0.72	0.47	0.57	0.62	0.86
Kim *et al.* (2015)	71.35	51.75	79.28	86.68	105.24
	0.15	0.49	0.33	0.35	0.48
	0.47	0.81	0.42	0.46	0.71

Note: Three values presented in each cell represent MAPE, RMSE, and R^2, respectively.

Table 14 | (a) Error analysis of different approaches in estimating *ds/y* in the LBS condition and selected ranges of *b/y*

Different approaches	$b/y < 0.25$	$0.25 \leq b/y < 0.5$	$0.5 \leq b/y < 1.0$	$1.0 \leq b/y < 1.5$
Present model (ANFIS)	24.38	13.67	11.92	13.68
	0.11	0.14	0.27	0.25
	0.30	0.81	0.84	0.35
Present model (GEP)	23.90	16.39	9.31	12.82
	0.09	0.14	0.15	0.18
	0.24	0.82	0.88	0.53
Colemon (1972)	24.88	22.16	7.41	19.02
	0.09	0.20	0.08	0.24
	0.43	0.80	0.86	0.42
Jain & Fischer (1979)	96.10	61.79	9.94	29.75
	0.28	0.30	0.14	0.39
	0.11	0.58	0.88	0.49
Johnson (1995)	18.46	11.78	9.48	56.66
	0.06	0.11	0.22	0.67
	0.59	0.85	0.84	0.57
Yanmaz (2001)	52.13	25.28	8.77	14.08
	0.15	0.14	0.05	0.22
	0.16	0.78	0.85	0.53

Yanmaz (2001) render less values of MAPE and RMSE. For $0.25 \leq Fr < 0.50$ and $0.75 \leq Fr < 1.0$, the present ANFIS model renders less error than other models. However, the present GEP model shows the least error for other ranges of *Fr* value.

Overall, the proposed ANFIS model shows better accuracy for both CWS and LBS and the GEP model shows better accuracy for certain definite input ranges of *b/y*, U/U_c, and *Fr* in the case of LBS and performed well over the other existing empirical models.

Table 14 | (b) Error analysis of different approaches in estimating *ds/y* in the LBS condition and selected ranges of U/U_c

Different approaches	$1 < U/U_c < 1.2$	$1.2 \leq U/U_c < 1.5$	$1.5 \leq U/U_c < 2.5$	$2.5 \leq U/U_c < 3.5$	$U/U_c \geq 3.5$
Present model (ANFIS)	21.59 0.20 0.61	14.74 0.14 0.86	17.39 0.22 0.86	18.31 0.28 0.87	22.10 0.35 0.53
Present model (GEP)	28.23 0.16 0.83	14.32 0.10 0.92	14.59 0.11 0.92	13.01 0.14 0.89	10.19 0.18 0.75
Colemon (1972)	33.42 0.15 0.85	15.47 0.15 0.85	16.19 0.13 0.90	15.45 0.16 0.88	19.48 0.27 0.68
Jain & Fischer (1979)	55.48 0.22 0.64	54.47 0.27 0.80	66.80 0.31 0.93	61.04 0.37 0.91	41.33 0.40 0.76
Johnson (1995)	31.01 0.22 0.86	28.88 0.31 0.86	19.03 0.26 0.91	17.97 0.29 0.88	14.96 0.30 0.68
Yanmaz (2001)	36.33 0.16 0.79	29.32 0.15 0.85	29.40 0.15 0.93	23.62 0.17 0.89	14.55 0.18 0.77

Note: Three values presented in each cell represent MAPE, RMSE, and R^2, respectively.

Table 14 | (c) Error analysis of different approaches in estimating *ds/y* in the LBS condition and selected ranges of *Fr*

Different approaches	$Fr < 0.25$	$0.25 \leq Fr < 0.50$	$0.50 \leq Fr < 0.75$	$0.75 \leq Fr < 1.0$	$Fr \geq 1.0$
Present model (ANFIS)	21.61 0.29 0.81	19.89 0.15 0.84	23.14 0.18 0.84	11.97 0.16 0.85	24.64 0.50 0.66
Present model (GEP)	22.73 0.16 0.84	14.28 0.11 0.90	15.74 0.10 0.90	13.32 0.15 0.86	14.30 0.22 0.75
Colemon (1972)	26.35 0.19 0.84	21.80 0.14 0.86	17.37 0.09 0.91	14.66 0.18 0.84	19.16 0.31 0.34
Jain & Fischer (1979)	41.65 0.27 0.68	56.19 0.25 0.75	79.30 0.33 0.93	34.98 0.34 0.86	33.98 0.41 0.39
Johnson (1995)	30.01 0.33 0.88	24.27 0.25 0.87	17.74 0.20 0.88	24.56 0.39 0.83	25.13 0.38 0.34
Yanmaz (2001)	14.30 0.17 0.81	26.42 0.12 0.86	39.20 0.16 0.92	13.82 0.15 0.84	19.88 0.26 0.40

Note: Three values presented in each cell represent MAPE, RMSE, and R^2, respectively.

CONCLUSIONS

In the present study, 442 and 213 data have been used for the modeling of clear-water and live-bed scour depth, respectively. The Gamma test reveals that pier diameter, flow depth, Froude number, approach flow velocity, critical flow velocity, geometric standard deviation, and median grain size are the most critical parameters to predict the scour depth at the bridge pier. In this study, for the prediction of clear-water and LBS depths through the ANFIS model, generalized bell membership

function (gbellmf) of size [22222] and Gaussian membership function (gaussmf) of size [33222] have been recommended, respectively. The coefficient of determination (R^2) value using normalized data was found to be 0.95 and 0.95 for clear-water and LBS, respectively. The MAPE value using normalized data was found to be less than 10 and 6% for clear-water and LBS, respectively.

In the GEP model for the prediction of scour depth in both clear-water and live-bed conditions, MSE fitness function and 30 chromosomes have been recommended. The coefficient of determination (R^2) value using normalized data was found to be 0.88 and 0.90 for clear-water and LBS, respectively. The MAPE value using normalized data was found to be less than 22 and 16% for clear-water and LBS, respectively. Comparison of the performance of the ANFIS model with a GEP model for the prediction of clear-water and LBS depth demonstrates that the ANFIS model is more accurate for CWS and GEP model is more accurate as evident from the error indices.

For different input ranges of b/y, U/U_c, and Fr, the ANFIS model was found to provide less error in terms of MAPE and RMSE and high R^2 value for CWS condition, however, in LBS condition, the GEP model was found to provide less error and high R^2 value for certain ranges of different input parameter.

The limitation of the present approach is the range of data sets used in modeling of CWS and LBS. The model will provide better results if the input parameter value lies in the same range as mentioned in Tables 3 and 4 respectively for CWS and LBS. Further research is needed to improve the accuracy of the model by incorporating the impact of bridge pier shapes.

DATA AVAILABILITY STATEMENT

All relevant data are available from an online repository or repositories. (https://drive.google.com/drive/folders/1fk1spzZP-2m4BsWG2R2jlERm0EvZMY1C?usp=share_link)

CONFLICT OF INTEREST

The authors declare there is no conflict.

REFERENCES

Agalbjorn, S., Koncar, N. & Jones, A. J. 1997 A note on the Gamma test. *Neural Computing and Applications* **5** (3), 131–133.

Aksoy, A. O., Bombar, G., Arkis, T. & Guney, M. S. 2017 Study of the time-dependent clear water scour around circular bridge piers. *Journal of Hydrology and Hydromechanics* **65** (1), 26–34.

Azmathullah, H. M., Deo, M. C. & Deolalikar, P. B. 2005 Neural networks for estimation of scour downstream of a ski-jump bucket. *Journal of Hydraulic Engineering* **131** (10), 898–908.

Bateni, S. M., Borghei, S. M. & Jeng, D. S. 2007 Neural network and neuro-fuzzy assessments for scour depth around bridge piers. *Engineering Applications of Artificial Intelligence* **20** (3), 401–414.

Breusers, H. N. C. & Raudkivi, A. J. 1991 *Scouring. IAHR Hydraulic Structures Design Manual 2*. AA Balkema, Rotterdam, The Netherlands.

Chabert, J. & Engeldinger, P. 1956 Study of scour around bridge piers. *Report Prepared for the Laboratoire National d'Hydraulique*.

Chee, R. K. W. 1982 *Live-bed Scour at Bridge Piers*. Auckland University, New Zealand. p. 290.

Chiew, Y. M. 1984 *Local Scour at Bridge Piers*. Auckland University, New Zealand.

Coleman, N. L. 1971 Analyzing laboratory measurements of scour at cylindrical piers in sand beds. In: *Proceedings of the 14th IAHR Congress: Hydraulic Research and its Impact on the Environment.* Paris, France, pp. 307–313.

Coleman, N. L. 1972 Analyzing laboratory measurements of scour at cylindrical piers in sand beds. In: *Hydraulic Research and its Impact on the Environment*.

Dang, N. M., Tran Anh, D. & Dang, T. D. 2021 ANN optimized by PSO and firefly algorithms for predicting scour depths around bridge piers. *Engineering with Computers* **37**, 293–303.

Das, B. S., Devi, K., Khuntia, J. R. & Khatua, K. K. 2020 Discharge estimation in converging and diverging compound open channels by using adaptive neuro-fuzzy inference system. *Canadian Journal of Civil Engineering* **47** (12), 1327–1344.

Devi, K., Das, B. S., Khuntia, J. R. & Khatua, K. K. 2021 Analytical solution for depth-averaged velocity and boundary shear in a compound channel. In: *Proceedings of the Institution of Civil Engineers-Water Management* **174** (3), 143–158.

Dey, S., Bose, S. K. & Sastry, G. L. 1995 Clear water scour at circular piers: A model. *Journal of Hydraulic Engineering* **121** (12), 869–876.

Durrant, P. J. 2001 *winGamma: A non-Linear Data Analysis and Modelling Tool with Applications to Flood Prediction*. Unpublished Ph. D. Thesis, Department of Computer Science, Cardiff University, Wales, UK.

Ebtehaj, I., Sattar, A. M., Bonakdari, H. & Zaji, A. H. 2017 Prediction of scour depth around bridge piers using self-adaptive extreme learning machine. *Journal of Hydroinformatics* **19** (2), 207–224.

Etemad-Shahidi, A., Bonakdar, L. & Jeng, D. S. 2015 Estimation of scour depth around circular piers: Applications of model tree. *Journal of Hydroinformatics* **17** (2), 226–238.

Ettema, R. 1976 *Influence of Bed Gradation on Local Scour*. University of Auckland, School of Engineering, New Zealand, No. 124. Report.
Ettema, R. 1980 *Scour at Bridge Piers.* Doctoral dissertation. University of Auckland, New Zealand.
Ettema, R., Nakato, T. & Valer-Ioan Muste, M. 2006 *An Illustrated Guide for Mnitoring and Protecting Bridge Waterways Against Scour*. No. Project TR-515. IIHR-Hydroscience & Engineering, University of Iowa.
Ettema, R., Melville, B. W. & Barkdoll, B. 1998 Scale effect in pier-scour experiments. *Journal of Hydraulic Engineering* **124** (6), 639–642.
Ferreira, C. 2002 Gene expression programming in problem solving. In: *Soft Computing and Industry*. (Roy, R., Köppen, M., Ovaska, S., Furuhashi, T. & Hoffmann, F. eds). Springer, London, pp. 635–653.
Ferreira, C. 2006 *Gene Expression Programming: Mathematical Modeling by an Artificial Intelligence*, Vol. 21. Springer, The Netherlands.
Firat, M. 2009 Scour depth prediction at bridge piers by ANFIS approach. In: *Proceedings of the Institution of Civil Engineers-Water Management* **162** (4), 279–288.
Firat, M. & Gungor, M. 2009 Generalized regression neural networks and feed forward neural networks for prediction of scour depth around bridge piers. *Advances in Engineering Software* **40** (8), 731–737.
Graf, W. H. 1995 *Load Scour Around Piers*. Annual Report. Laboratorie de Recherches Hydrauliques, Ecole Polytechnique Federale de Lausanne, Lausanne, Switzerland.
Guven, A. & Aytek, A. 2009 New approach for stage–discharge relationship: Gene-expression programming. *Journal of Hydrologic Engineering* **14** (8), 812–820.
Hamidifar, H., Zanganeh-Inaloo, F. & Carnacina, I. 2021 Hybrid scour depth prediction equations for reliable design of bridge piers. *Water* **13** (15), 2019.
Hsu, C. W., Chang, C. C. & Lin, C. J. 2003 *A Practical Guide to Support Vector Classification*, Technical Report, Department of Computer Science and Information Engineering, University of National Taiwan, Taipei, pp. 1–16.
Jain, S. C. & Fischer, E. E. 1979 *Scour Around Circular Bridge Piers at High Froude Numbers (No. FHWA-RD-79-104 Final Rpt)*.
Jang, J. S. R. 1991 Fuzzy modeling using generalized neural networks and Kalman filter algorithm. In: *Proceedings of the Ninth National Conference on Artificial Intelligence*, 14–19 July 1991. Anaheim, Calif., pp. 762–767.
Jang, J. S. 1993 ANFIS: Adaptive-network-based fuzzy inference system. *IEEE Transactions on Systems, man, and Cybernetics* **23** (3), 665–685.
Jang, J. S. R., Sun, C. T. & Mizutani, E. 1997 *Neuro-Fuzzy and Soft Computing: A 669 Computational Approach to Learning and Machine Intelligence*. Prentice- Hall 670 International, London.
Johnson, P. A. 1995 Comparison of pier-scour equations using field data. *Journal of Hydraulic Engineering* **121** (8), 626–629.
Kaya, A. 2010 Artificial neural network study of observed pattern of scour depth around bridge piers. *Computers and Geotechnics* **37** (3), 413–418.
Khan, M., Azamathulla, H. M. & Tufail, M. 2012 Gene-expression programming to predict pier scour depth using laboratory data. *Journal of Hydroinformatics* **14** (3), 628–645.
Khan, M., Tufail, M., Ajmal, M., Haq, Z. U. & Kim, T. W. 2017 Experimental analysis of the scour pattern modeling of scour depth around bridge piers. *Arabian Journal for Science and Engineering* **42**, 4111–4130.
Khuntia, J. R., Devi, K. & Khatua, K. K. 2019 Flow distribution in a compound channel using an artificial neural network. *Sustainable Water Resources Management* **5** (4), 1847–1858.
Kim, I., Fard, M. Y. & Chattopadhyay, A. 2015 Investigation of a bridge pier scour prediction model for safe design and inspection. *Journal of Bridge Engineering* **20** (6), 04014088.
Kothyari, U. C., Garde, R. C. J. & Ranga Raju, K. G. 1992 Temporal variation of scour around circular bridge piers. *Journal of Hydraulic Engineering* **118** (8), 1091–1106.
Kumar, A., Kothyari, U. C. & Raju, K. G. R. 2012 Flow structure and scour around circular compound bridge piers – A review. *Journal of Hydro-Environment Research* **6** (4), 251–265.
Kumar, S., Khuntia, J. R., Devi, K., Das, B. S. & Khatua, K. K. 2023 Closure to 'Prediction of flow resistance in an open channel over movable beds using artificial neural network' by Satish Kumar, Jnana Ranjan Khuntia, and Kishanjit Kumar Khatua. *Journal of Hydrologic Engineering* **28** (2), 07022012.
Laursen, E. M. 1963 An analysis of relief bridge scour. *Journal of the Hydraulics Division* **89** (3), 93–118.
Melville, B. W. 1997 Pier and abutment scour: An integrated approach. *Journal of Hydraulic Engineering* **123** (2), 125–136.
Melville, B. W. & Chiew, Y. M. 1999 Time scale for local scour at bridge piers. *Journal of Hydraulic Engineering* **125** (1), 59–65.
Melville, B. W. & Coleman, S. E. 2000 *Bridge Scour*. Water Resource Publications, LLC, Littleton, CO, USA.
Miller, M. C., McCave, I. N. & Komar, P. 1977 Threshold of sediment motion under unidirectional currents. *Sedimentology* **24** (4), 507–527.
Mueller, D. S. 1996 *Local Scour at Bridge Piers in Nonuniform Sediment Under Dynamic Conditions*. PhD Dissertation, Colorado State University, Fort Collins, CO.
Muzzammil, M. & Ayyub, M. 2010 ANFIS-based approach for scour depth prediction at piers in non-uniform sediments. *Journal of Hydroinformatics* **12** (3), 303–317.
Neill, C. R. 1973 *Guide to Bridge Hydraulics, Roads and Transportation, Association of Canada*. University of Toronto Press, Toronto.
Nil, B. A. & Das, B. S. 2023 Clear water and live bed scour depth modelling around bridge pier using support vector machine. *Canadian Journal of Civil Engineering.* (in press). doi:10.1139/cjce-2022-0237.
Noori, R., Karbassi, A. R., Moghaddamnia, A., Han, D., Zokaei-Ashtiani, M. H., Farokhnia, A. & Gousheh, M. G. 2011 Assessment of input variables determination on the SVM model performance using PCA, Gamma test, and forward selection techniques for monthly stream flow prediction. *Journal of Hydrology* **401** (3–4), 177–189.

Pal, M., Singh, N. K. & Tiwari, N. K. 2011 Support vector regression-based modeling of pier scour using field data. *Engineering Applications of Artificial Intelligence* **24** (5), 911–916.

Pandey, M., Sharma, P. K., Ahmad, Z. & Karna, N. 2018 Maximum scour depth around bridge pier in gravel bed streams. *Natural Hazards* **91** (2), 819–836.

Pandey, M., Oliveto, G., Pu, J. H., Sharma, P. K. & Ojha, C. S. P. 2020a Pier scour prediction in non-uniform gravel beds. *Water* **12** (6), 1696.

Pandey, M., Zakwan, M., Khan, M. A. & Bhave, S. 2020b Development of scour around a circular pier and its modelling using genetic algorithm. *Water Supply* **20** (8), 3358–3367.

Raikar, R. V. & Dey, S. 2005 Clear-water scour at bridge piers in fine and medium gravel beds. *Canadian Journal of Civil Engineering* **32** (4), 775–781.

Raudkivi, A. J. & Ettema, R. 1983 Clear water scour at cylindrical piers. *Journal of Hydraulic Engineering.* **109** (3), 338–350.

Shamshirband, S., Mosavi, A. & Rabczuk, T. 2020 Particle swarm optimization model to predict scour depth around a bridge pier. *Frontiers of Structural and Civil Engineering* **14**, 855–866.

Sharafati, A., Haghbin, M., Motta, D. & Yaseen, Z. M. 2021 The application of soft computing models and empirical formulations for hydraulic structure scouring depth simulation: A comprehensive review, assessment and possible future research direction. *Archives of Computational Methods in Engineering* **28**, 423–447.

Sharafi, H., Ebtehaj, I., Bonakdari, H. & Zaji, A. H. 2016 Design of a support vector machine with different kernel functions to predict scour depth around bridge piers. *Natural Hazards* **84**, 2145–2162.

Shen, H. W., Schneider, V. R. & Karaki, S. 1969 Local scour around bridge piers. *Journal of the Hydraulics Division* **95**. https://doi.org/10.1061/JYCEAJ.0002197.

Sheppard, D. M., Odeh, M. & Glasser, T. 2004 Large scale clear-water local pier scour experiments. *Journal of Hydraulic Engineering* **130** (10), 957–963.

Shin, J. H. & Park, H. I. 2010 Neural network formula for local scour at piers using field data. *Marine Georesources and Geotechnology* **28** (1), 37–48.

Sheppard, D. M. & Miller, W. 2006 Live-bed local pier scour experiments. *Journal of Hydraulic Engineering* **132** (7), 635–642.

Sreedhara, B. M., Patil, A. P., Pushparaj, J., Kuntoji, G. & Naganna, S. R. 2021 Application of gradient tree boosting regressor for the prediction of scour depth around bridge piers. *Journal of Hydroinformatics* **23** (4), 849–863.

Toth, E. & Brandimarte, L. 2011 Prediction of local scour depth at bridge piers under clear-water and live-bed conditions: Comparison of literature formulae and artificial neural networks. *Journal of Hydroinformatics* **13** (4), 812–824.

Tsui, A. P., Jones, A. J. & De Oliveira, A. G. 2002 The construction of smooth models using irregular embeddings determined by a Gamma test analysis. *Neural Computing & Applications* **10** (4), 318–329.

Yanmaz, M. A. 2001 Uncertainty of local scour parameters around bridge piers. *Journal Engineering and Environmental Science* **25**, 127–137.

Yanmaz, A. M. & Altinbilek, H. D. G. A. 1991 Study of time-dependent local scour around bridge piers. *Journal of Hydraulic Engineering* **117** (10), 1247–1268.

First received 7 December 2022; accepted in revised form 20 April 2023. Available online 5 May 2023